Spin orientation switching in layered perovskite oxyfluoride $Pb_3Fe_2O_5F_2$

Kengo Oka (koka@apch.kindai.ac.jp)
Kindai University https://orcid.org/0000-0002-1800-8575
Yusuke Nambu
Tohoku University https://orcid.org/0000-0003-1167-7124
Masayuki Ochi
Osaka University
Naoaki Hayashi
Osaka Prefecture University
Yoshihiro Kusano
Okayama University of Science https://orcid.org/0000-0003-3646-3413
Takuya Aoyama
Tohoku University
Yui Ishii
Osaka Prefecture University
Kazuhiko Kuroki
Osaka University
Shigeo Mori
Osaka Prefecture University
Mikio Takano
Research Institute for Production Development
Mitsunobu Iwasaki
Kindai University
Naoki Noma
Kindai University
Hiroshi Kageyama
Kyoto University https://orcid.org/0000-0002-3911-9864

Article

Keywords: magnetic materials, spin alignment, layered perovskite oxyfluoride Pb3Fe2O5F2

Posted Date: July 29th, 2021

DOI: https://doi.org/10.21203/rs.3.rs-678519/v1

Abstract

Control of spin alignment in magnetic materials is crucial for developing switching devices. In molecular magnets, magnetic anisotropy can be rationally controlled by varying their ligands that allow tuning of ligand field splitting energy. However, the inherent weak magnetic interaction between spins or spin-cluster results in spin reorientation (SR) occurring only at low temperatures. Here, we show that layered perovskite oxyfluoride $Pb_3Fe_2O_5F_2$ exhibits a SR transition at 380 K, with the magnetic moments changing from perpendicular to parallel to the *c*-axis. It is found that the SR is caused by a ferroelectric-like phase transition, where the magnetic HOMO-LUMO interaction changes upon the structural transition due to the concerted effect of the heteroleptic FeO_5F coordination and the steric effect of Pb. This finding indicates that the design of spin orientation by local coordination environment, which is common in molecular magnets, can be extended to extended oxides by introducing different anions.

Introduction

Controlling the spin orientation, or magnetic anisotropy, in magnetic materials is an essential issue for applications such as magnetic switching devices. For molecular magnets, magnetic anisotropy arises mainly from spin-orbit interaction, thus the most promising and rational approach is to tailor the crystalline field splitting energy using various ligands around a magnetic metal center, as demonstrated in single molecule magnets (SMMs).[1–7] Magnetic anisotropy in molecular magnets is theoretically explained by magnetic exchange interaction and ligand field splitting, as applied to Mn_{12}-acetate, $[Fe_8O_2(OH)_{12}(tacn)_6]$[8] and Mn(II)-[3 x 3] grid[9]. Magnetic anisotropy phase diagrams for $[PPh_4][Ln\{Pt(SAc)_4\}_2]$ (*Ln* = Ho, Er) have been reproduced as a function of temperature, magnetic field, and pressure.[7] Despite the tunability and predictable magnetic anisotropy in SMMs, the switching behavior occurs at low temperatures, thereby limiting their applications.

Extended solid-state materials, such as oxides, have an advantage over SMMs in terms of higher operating temperatures, which allows for the operation of magnetic devices at room temperature. Unlike SMMs, magnetic interactions are mediated by magnetic ions on infinite magnetic lattices, and long-range magnetic orders such as ferromagnetic and antiferromagnetic states occur depending on the crystal structure and magnetic interactions. However, the local coordination environments around magnetic ion are mostly homoleptic, and limited changes in coordinates do not allow for extensive tuning of crystal filed observed in SMMs. Although some oxides exhibit spin reorientation (SR) as a function of temperature and pressure, the underlying mechanism is far more complex, compared to molecular magnets. For example, the SR transition observed perovskite-based materials, $LnFeO_3$ (Ln: Yb, Sm, Er, Tm, Dy)[10–15] and $MnNdMnSbO_6$,[16] and $Mn_2(Fe_{0.8}Mo_{0.2})MoO_6$[17] are attributed to the subtle competition between two magnetic sublattices (e.g., Ln- and Fe-sublattices in $LnFeO_3$).

Mixed anion compounds have recently been attracting attention as materials that produce structures and functions not found in oxides [18]. In particular, the heteroleptic coordination around a metal center may

allow for the intensive tuning of crystal field splitting, as seen in molecular magnets. In this study, we show that layered perovskite oxyfluoride $Pb_3Fe_2O_5F_2$ exhibits SR above room temperature through a structural transition similar to a ferroelectric transition. As shown schematically illustrated in Fig. 1, this phase transition drastically changes the heteroleptic coordination environment around Fe^{3+} ion and alters the crystal field splitting. This study demonstrates a new possibility in rationally designing magnetic anisotropy of extended solid materials to explore SR at high temperatures.

Results And Discussions

Powder sample of $Pb_3Fe_2O_5F_2$ was prepared using the solid-state reaction by heating a mixture of PbO, PbF_2, and Fe_2O_3 at 600°C for 12 hours in a vacuum. The X-ray diffraction (XRD) data indicated the formation of a double-layered ($n = 2$) Ruddlesden-Popper (RP) perovskite (see Supplementary Fig. 1). While related oxyfluorides, $Sr_3Fe_2O_6F_{0.87}$[19] and $Sr_3Fe_2O_{5.44}F_{1.56}$,[20] adopt an ideal tetragonal RP structure, the synchrotron X-ray diffraction (SXRD) profile at 100 K for $Pb_3Fe_2O_5F_2$ was assigned by a monoclinic cell ($a = 3.9406(1)$ Å, $b = 3.9416(1)$ Å, $c = 21.4002(2)$ Å, and $\gamma = 89.816(1)$ °). The structural distortion in perovskite is rationalized using the tolerance factor t,[21], but the t value for $Pb_3Fe_2O_5F_2$ is almost unity ($t = 0.98 \sim 1.00$)[21], suggesting that the lowered symmetry arises from the stereochemical effect of Pb^{2+}.

The temperature evolution of the SXRD patterns (Fig. 2a) revealed a structural transition, where the unit cell of the high-temperature (HT) phase is given by $2a_p \times 2b_p \times c_p$, relative to the primitive cell ($a_p \times b_p \times c_p$) in the low-temperature (LT) phase. A two-phase coexistence in a wide temperature range (380–400 K on heating and 400 – 320 K on cooling) indicates a first-order nature of the transition, as supported by the magnetic susceptibility (Fig. 2c, top). The normalized cell parameters show an anisotropic thermal expansion, with a pronounced c-axis reduction with cooling across the phase boundary (Fig. 2c, middle).

^{57}Fe-Mössbauer spectra at 500 K and 78 K (Fig. 2b) consist of a paramagnetic doublet and a magnetic sextet, with linewidths of 0.38 mm/s and 0.31 mm/s, respectively. The nearly resolution-limited spectra are in sharp contrast with the cubic perovskite oxyfluorides,[22,23] where anionic-site disorder causes spectrum broadening. For the RP oxyfluorides, anion-disordered $Sr_3Fe_2O_{5-x}F_{2-y}$ and Sr_2FeO_3F have broad peaks, while anion-ordered Sr_2FeO_3F has a resolution-limited spectrum.[24] These observations indicate that $Pb_3Fe_2O_5F_2$ has a single iron site, with a full O/F anion order. A hyperfine field (HF) of 53.5 T and an isomer shift (IS) of 0.51 mm/s at 78 K (Supplementary Table 1) are typical of the high-spin Fe^{3+}, in agreement with the composition. A steep increase in the magnetic susceptibility below 490 K (Fig. 2c, top) indicates a canted antiferromagnetic transition in the HT region (Supplementary Fig. 2).

For the LT phase, the extinction reflection conditions (Supplementary Fig. 3) and the single-site occupancy of Fe (Fig. 2b) uniquely gave $P2_1/m$ space group. Since O and F atoms are indistinguishable by X-ray, we performed Rietveld refinement of the SXRD data at 100 K using a Pb_3Fe_2"O_7" composition (Fig. 3a, Supplementary Table 2). The bond valence sum (BVS) of "oxygen" using the tabulated

parameters[25] gave acceptable values for the equatorial (O1: 2.03, O2: 2.06) and the bridging (O3: 1.88) sites, while the apical (O4) site has a significantly smaller value of 1.17. Thus, we conclude that the O4 site is selectively occupied by the fluorine anion. For the HT phase, the reflection conditions (Fig. 3b) uniquely gave $P4_2/nbc$, and the BVS calculation using the refined structure (R_{WP} = 6.57% and R_I = 4.89%) again supported the selective occupation of F^- at the apical site (Supplementary Table 2).

The appearance of the superstructure ($2a_p \times 2b_p \times c_p$) in the HT phase appears unusual, but the same behavior has been seen in, e.g., $BiFeO_3$,[26] $BiCoO_3$,[27] and $BiZn_{0.5}V_{0.5}O_3$[28] where a ferroelectric-to-paraelectric transition takes place upon heating or applying pressures. Such behavior in $Pb_3Fe_2O_5F_2$ can be seen by comparing the FeO_2 plane in the two phases (Fig. 3). For the HT phase, the staggered alignment of oxide ions along the *b* axis looks responsible for the $2a_p \times 2b_p \times c_p$ supercell. In contrast, the LT phase shows a uniform displacement, thus removing the superstructure while inducing a large electronic polarization along the *b* axis. Note that the antiparallel stacking of the FeO_2 layers cancels out the total electric polarization. Thus, the structural transition in $Pb_3Fe_2O_5F_2$ can be considered to originate from the steric effect of $6s^2$ lone pair electrons of Pb^{2+}.

As typified by the multiferroic $BiFeO_3$, the steric effect of Bi^{3+} and the magnetic moment of Fe^{3+} may lead to interesting phenomena induced by the structural phase transition. Neutron powder diffraction (NPD) pattern at 400 K exhibits magnetic reflections given by a propagation vector of k = (0, 0, 0), corresponding to $(1/2, 1/2, 0)_p$ in the reduced cell. The Fe magnetic moment increases with decreasing temperature, giving 3.5(1) m_B/Fe at 4 K. Magnetic structure refinement with group-theoretical analysis (see Supplementary Information) revealed the G-type antiferromagnetic order, with magnetic moments being perpendicular to the *c* axis. This spin orientation is consistent with the Mössbauer results (Supplementary Table 1). Most notably, the relative intensity of the magnetic peaks drastically changes; the intensity ratio of I_{112}/I_{113} is 0.32 at 400 K, but it is reduced to 1.78 at 4 K (Fig. 4). This observation strongly indicates that the magnetic moments at 4 K align parallel and antiparallel to the *c* axis since magnetic neutron scattering can detect spin components perpendicular to the momentum transfer. Indeed, the group-theoretical analysis confirms the SR by comparing the reliable factor through magnetic structure refinements. Thus, the structural transition drives the spin orientation change from perpendicular to parallel to the *c* axis.

As mentioned earlier, SR has been observed in extended solids, but its origin is rather complicated. SR in bulk a-Fe_2O_3, known as Morin transition, has been interpreted as originating from the competition between crystalline-, shape- and surface magnetic anisotropy.[29] For other bulk compounds, it is mostly caused by the coupling between two magnetic sublattices, as found in $Ln_2Fe_{14}B$,[10–15] $LnFeO_3$ (*Ln* = magnetic lanthanides),[30–38] $MnNdMnSbO_6$,[16] and $Mn_2(Fe_{0.8}Mo_{0.2})MoO_6$,[17] with different magnetic sublattices (e.g., *Ln*-4*f vs*. Fe-3*d* in $LnFeO_3$). In these examples, the magnetic order of each sublattice occurs at different temperatures, and the spin orientation of the sublattice with a higher transition temperature (Fe-3*d*) changes when another sublattice (*Ln*-4*f*) is ordered upon cooling, indicating that a

subtle competition between different sublattices is at play. Other examples include $BaFeO_3$ with charge disproportionation of Fe ions,[39] $Ba_{0.65}Na_{0.35}Fe_2As_2$ with competing antiferromagnetic and superconducting phases.[40–42] The SRs in all of these materials involve strong correlations of electrons.

In contrast to the extended solids shown above, the SR in $Pb_3Fe_2O_5F_2$ is driven by the ferroelectric like phase transition in the perovskite layers of FeO_5F octahedra. As seen in Fig. 5, Fe is located approximately at the center of the four equatorial oxygens in the HT phase, but is substantially off-centered in the LT phase. This significant distortion in the LT phase is expected to stabilize the d_{x2-y2} orbital, one of the antibonding orbitals, due to the drastic decrease in the overlap of the O 2p orbitals.

According to Whangbo *et al.*,[43] magnetic anisotropy in extended solids can be predictable by considering the orbitals responsible for magnetic HOMO-LUMO interactions, i.e., the crystal field splitting of *d*-orbitals. We employ this model to understand the SR in $Pb_3Fe_2O_5F_2$. Given high-spin state of Fe^{3+} and the Mott insulating nature, the e_g orbital as HOMO, we consider magnetic HOMO-LUMO interaction between e_g (HOMO: parallel spins) and t_{2g} (LUMO: anti-parallel spins) orbitals (Supplementary Fig. 5). From the observed spin orientation, the difference in magnetic HOMO-LUMO states (L values) for in-plane ($\perp c$, HP) and perpendicular ($// c$, LT) spin orientations should be given by $|\Delta L_Z| = 0$ and $|\Delta L_Z| = 1$, respectively. Since the $|\Delta L_Z| = 0$ interaction at HP is possible only for d_{x2-y2} (HOMO) and d_{xy} (LUMO) orbitals, magnetic HOMO is expected to change from d_{x2-y2} (HT phase) to d_{3z2-r2} (LT phase).

To verify this scenario, we performed first-principles calculations using density functional theory. The partial density of states (DOS) of Fe^{3+} in Fig. 6a indicates that the magnetic HOMO changes from the d_{x2-y2} band in the HT phase to a mixed band of d_{x2-y2} and d_{3z2-r2} orbitals in the LT phase. The magnetic LUMO is composed of the t_{2g} orbitals (d_{xy}, d_{yz}, d_{xz}) in both phases. This result is consistent with our scenario because in the HT phase has a larger contribution of the d_{x2-y2} (HOMO) and d_{xy} (LUMO) orbitals, responsible for $|\Delta L_Z| = 0$ as shown in Fig. 6b. Thus, the change in magnetic HOMO is intuitively understood simply through the local coordination environment around Fe^{3+}. The magnetic HOMO in the HT phase can be understood as a strong repulsion of electrons in the d_{x2-y2} orbital from O 2p orbitals and a weak repulsion of the d_{3z2-r2} orbital because one of the apical anions being monovalent (see Fig .1). On the other hand, the LT phase has a stabilized d_{x2-y2} orbital, which increase the contribution of d_{3z2-r2} orbital to magnetic HOMO.

In molecular magnets including SMMs, control of magnetic anisotropy by tuning orbital splitting has been achieved using a variety of ligands.[6] However, while the nearly isolated spins (or clusters) simplify the interpretation of spin orientation, the weak magnetic interaction between spins (or spin clusters) inevitably lowers the temperature at which the magnetic anisotropy changes. For example, $[Mn_{12}O_{12}(OAc)_{16}(H_2O)_4]$[44] shows magnetic hysteresis only below 4 K. For most of SMMs, ferromagnetic like behavior is seen below 20 K.[1,45] A hexatert-butyldysprosocenium complex shows magnetic hysteresis around 60 K, which is the highest transition temperature.[46,47]

In marked contrast, $Pb_3Fe_2O_5F$ has the magnetic transition temperature of 490 K and the structural phase transition (and SR) of 380 K, both far beyond room temperature. Given the ferroelectric-like nature of structural transition, the operating temperature might be widely tuned by, e.g., non-magnetic substitution of Pb. $Pb_3Fe_2O_5F$ is a mixed-anion compound, which, as is the case with SMMs, allows the crystal field to be controlled by different ligands to a degree greater than is possible with oxides. Furthermore, the combination of the steric effects of the heteroleptic coordination and lone pair electrons can induce a dramatic change in the ligand field with temperature. These two factors are considered to be essential for temperature-induced SR, and hence it would be possible to search for other materials that satisfy these requirements.

Methods

Powder sample of $Pb_3Fe_2O_5F_2$ was prepared through the solid-state reaction using a stoichiometric mixture of PbO (99.9%, Raremetallic Co.), PbF_2 (99.9%, Raremetallic Co.), and α-Fe_2O_3 (99.9%, Raremetallic Co.) powders. The pelletised mixture was placed in a Pt crucible, sealed in an evacuated Pyrex tube, and reacted at 873 K for 12 h.

Synchrotron X-ray diffraction (SXRD) patterns were collected at the beamline BL02B2 of SPring-8[48] and refined by the Rietveld method using the RIETAN-FP program.[49] The SXRD patterns were collected in transmission geometry using a solid state detector. The sample powders were each sealed in glass capillaries and rotated during measurement. The incident beam was monochromatized to λ = 0.41967 Å.

Neutron powder diffraction data were collected on HB-2A POWDER installed at High Flux Isotope Reactor, Oak Ridge National Laboratory, USA, with λ = 1.5366 Å and 2.4068 Å. We collected diffraction patterns between T = 4 K and 600 K in a closed-cycle refrigerator. We employed group theoretical analysis to identify magnetic structures that are allowed by symmetry (see Supplementary Information for details).

The cross-sectional microstructure and electron diffraction patterns of the $Pb_3Fe_2O_5F_2$ sample were observed using transmission electron microscopy (TEM, JEOL JEM-2100F and JEM-2800) with energy-dispersive X-ray spectroscopy (EDS) after thinning by Ar ion milling at room temperature. Simulations of ED patterns were carried out using the multislice simulation software MacTempas.

We collected ^{57}Fe Mössbauer spectra using a ^{57}Co/Rh source and control absorber α-Fe. Magnetic properties were measured with a superconducting quantum interference device (SQUID) magnetometer (MPMS-XL, Quantum Design) equipped with an oven option for high temperatures.

First principles calculations were performed on the basis of the density functional theory. Since we perturbatively interpreted the spin-orbit coupling for understanding the magnetic anisotropy, the energy levels used in our discussion as the non-perturbative states were calculated without including the spin-orbit coupling (see Supplementary Information for details).

Declarations

Acknowledgements

We thank Dr. Stuart Calder of Oak Ridge National Laboratory for his help in the neutron diffraction measurement and Prof. Ko Mibu and Tomoko Onoue of Nagoya Institute of Technology for their help in the ^{57}Fe Mössbauer spectroscopy. This work was supported by a Grant-in-Aid for Scientific Research on Innovative Area “Mixed Anion (Project, 16K21724, 17H05473, 17H05481, 17H05487, 17H05489, 19H04704, 19H04683, 19H04697, 19H04706, 19K05655)” (JSPS). It was also partially supported by a Grant-in-Aids for Scientific Research (C) (Project JP16K05731). The synchrotron radiation experiments were performed at the BL02B2 of SPring-8 with the approval of the Japan Synchrotron Radiation Research Institute (JASRI) (Proposal No. 2018A1227, and 2018B1222). The neutron diffraction experiment was performed on HB-2A at High Flux Isotope Reactor, Oak Ridge National Laboratory, USA (Proposal No. IPTS-18713). The neutron powder diffraction study was performed under the GIMRT Program of the Institute for Materials Research, Tohoku University (Proposal No. 19N0007). The ^{57}Fe Mössbauer spectroscopy was supported by Nanotechnology Platform Program of MEXT, Grant Number JPMXP09S17NI39. The magnetic measurement using SQUID magnetometer was carried out under the Visiting Researcher's Program of the Institute for Solid State Physics, the University of Tokyo.

Author Contributions

K. O. and H. K. designed the research. K. O. carried out the samples preparation, SXRD, NPD and magnetic measurements. Y. N. analysed NPD patterns and wrote the NPD part. M. O. and K. K. performed first-principles calculations. N. H. and M. T. carried out ^{57}Fe Mössbauer spectroscopy and data analysis. Y. K., Y. I. and S. M. carried out ED study. T. A. carried out electronic measurements. N. N. and M. I discussed and interpreted the result. K. O. and H. K. prepared the manuscript as corresponding authors.

Competing Interests statement

There are no competing interests in the manuscript.

References

1 Woodruff, D. N., Winpenny, R. E. P. & Layfield, R. A. Lanthanide Single-Molecule Magnets. *Chem. Rev.* **113**, 5110-5148, doi:10.1021/cr400018q (2013).

2 Liddle, S. T. & van Slageren, J. Improving f-element single molecule magnets. *Chem. Soc. Rev.* **44**, 6655-6669, doi:10.1039/C5CS00222B (2015).

3 Craig, G. A. & Murrie, M. 3d single-ion magnets. *Chem. Soc. Rev.* **44**, 2135-2147, doi:10.1039/C4CS00439F (2015).

4 Cucinotta, G. *et al.* Magnetic Anisotropy in a Dysprosium/DOTA Single-Molecule Magnet: Beyond Simple Magneto-Structural Correlations. *Angew. Chem. Int. Ed.* **51**, 1606-1610, doi:10.1002/anie.201107453 (2012).

5 Perfetti, M. & Bendix, J. Descriptors of magnetic anisotropy revisited. *Chem. Commun.* **54**, 12163-12166, doi:10.1039/C8CC05756G (2018).

6 Perfetti, M. *et al.* Magnetic Anisotropy Switch: Easy Axis to Easy Plane Conversion and Vice Versa. *Adv. Funct. Mater.* **28**, 1801846, doi:10.1002/adfm.201801846 (2018).

7 Perfetti, M. & Bendix, J. The Multiple Faces, and Phases, of Magnetic Anisotropy. *Inorg. Chem.* **58**, 11875-11882, doi:10.1021/acs.inorgchem.9b00636 (2019).

8 Postnikov, A. V., Kortus, J. & Pederson, M. R. Density functional studies of molecular magnets. *Phys. status solidi* **243**, 2533-2572, doi:https://doi.org/10.1002/pssb.200541490 (2006).

9 Waldmann, O., Zhao, L. & Thompson, L. K. Field-Dependent Anisotropy Change in a Supramolecular Mn(II)- [3 × 3] Grid. *Phys. Rev. Lett.* **88**, 066401, doi:10.1103/PhysRevLett.88.066401 (2002).

10 Burlet, P., Coey, J. M. D., Gavigan, J. P., Givord, D. & Meyer, C. A note on exchange and crystal field interactions in $R_2Fe_{14}B$ compounds: $Yb_2Fe_{14}B$. *Solid State Commun.* **60**, 723-727, doi:https://doi.org/10.1016/0038-1098(86)90430-8 (1986).

11 Abache, C. & Oesterreicher, J. Magnetic anisotropies and spin reorientations of $R_2Fe_{14}B$-type compounds. *J. Appl. Phys.* **60**, 3671-3679, doi:10.1063/1.337574 (1986).

12 Yelon, W. B. & Herbst, J. F. Neutron scattering studies of the spin reorientation in $Er_2Fe_{14}B$. *J. Appl. Phys.* **59**, 93-96, doi:10.1063/1.336845 (1986).

13 Hirosawa, S. *et al.* Magnetization and magnetic anisotropy of $R_2Fe_{14}B$ measured on single crystals. *J. Appl. Phys.* **59**, 873-879, doi:10.1063/1.336611 (1986).

14 Piqué, C., Burriel, R. & Bartolomé, J. Spin reorientation phase transitions in $R_2Fe_{14}B$ (R = Y, Nd, Ho, Er, Tm) investigated by heat capacity measurements. *J. Magn. Magn. Mater.* **154**, 71-82, doi:https://doi.org/10.1016/0304-8853(95)00571-4 (1996).

15 García, L. M., Chaboy, J., Bartolomé, F. & Goedkoop, J. B. Orbital Magnetic Moment Instability at the Spin Reorientation Transition of $Nd_2Fe_{14}B$. *Phys. Rev. Lett.* **85**, 429-432, doi:10.1103/PhysRevLett.85.429 (2000).

16 Solana-Madruga, E. *et al.* Double Double Cation Order in the High-Pressure Perovskites MnRMnSbO_6. *Angew. Chem. Int. Ed.* **55**, 9340-9344, doi:10.1002/anie.201603526 (2016).

17 Li, M.-R. *et al.* $Mn_2(Fe_{0.8}Mo_{0.2})MoO_6$: A Double Perovskite with Multiple Transition Metal Sublattice Magnetic Effects. *Chem. Mater.* **30**, 4508-4514, doi:10.1021/acs.chemmater.8b00250 (2018).

18 Kageyama, H. *et al.* Expanding frontiers in materials chemistry and physics with multiple anions. *Nat. Commun* **9**, 772, doi:10.1038/s41467-018-02838-4 (2018).

19 Simon Case, G. *et al.* Syntheses, powder neutron diffraction structures and Mössbauer studies of some complex iron oxyfluorides: $Sr_3Fe_2O_6F_{0.87}$, Sr_2FeO_3F and $Ba_2InFeO_5F_{0.68}$. *J. Mater. Chem.* **9**, 2821-2827, doi:10.1039/A905730G (1999).

20 Tsujimoto, Y. *et al.* Topotactic Synthesis and Crystal Structure of a Highly Fluorinated Ruddlesden–Popper-Type Iron Oxide, $Sr_3Fe_2O_{5+x}F_{2-x}$ ($x \approx 0.44$). *Chem. Mater.* **23**, 3652-3658, doi:10.1021/cm201075g (2011).

21 Tilley, R. J. D. Perovskites: Structure-Property Relationships. *Wiley* (2016).

22 Inaguma, Y. *et al.* Structure and Mossbauer studies of F-O ordering in antiferromagnetic perovskite $PbFeO_2F$. *Chem. Mater.* **17**, 1386-1390, doi:10.1021/cm048125g (2005).

23 Takeiri, F. *et al.* $AgFeOF_2$: A Fluorine-Rich Perovskite Oxyfluoride. *Inorg. Chem.* **57**, 6686-6691, doi:10.1021/acs.inorgchem.8b00500 (2018).

24 Tsujimoto, Y., Matsushita, Y., Hayashi, N., Yamaura, K. & Uchikoshi, T. Anion Order-to-Disorder Transition in Layered Iron Oxyfluoride Sr_2FeO_3F Single Crystals. *Cryst. Growth Des.* **14**, 4278-4284, doi:10.1021/cg500484e (2014).

25 Brown, I. D. & Altermatt, D. Bond-valence parameters obtained from a systematic analysis of the Inorganic Crystal Structure Database. *Acta Crystallogr. B* **41**, 244-247, doi:doi:10.1107/S0108768185002063 (1985).

26 Belik, A. A., Yusa, H., Hirao, N., Ohishi, Y. & Takayama-Muromachi, E. Structural Properties of Multiferroic $BiFeO_3$ under Hydrostatic Pressure. *Chem. Mater.* **21**, 3400-3405, doi:10.1021/cm901008t (2009).

27 Oka, K. *et al.* Pressure-Induced Spin-State Transition in $BiCoO_3$. *J. Am. Chem. Soc.* **132**, 9438-9443, doi:10.1021/ja102987d (2010).

28 Yu, R. *et al.* New $PbTiO_3$-Type Giant Tetragonal Compound Bi_2ZnVO_6 and Its Stability under Pressure. *Chem. Mater.* **27**, 2012-2017, doi:10.1021/cm504133e (2015).

29 Hill, A. H. *et al.* Neutron Diffraction Study of Mesoporous and Bulk Hematite, α-Fe_2O_3. *Chem. Mater.* **20**, 4891-4899, doi:10.1021/cm800009s (2008).

30 Pierce, R. D., Wolfe, R. & Uitert, L. G. V. Spin Reorientation in Mixed Samarium-Dysprosium Orthoferrites. *J. Appl. Phys.* **40**, 1241-1242, doi:10.1063/1.1657611 (1969).

31 White, R. L. Review of Recent Work on the Magnetic and Spectroscopic Properties of the Rare-Earth Orthoferrites. *J. Appl. Phys.* **40**, 1061-1069, doi:10.1063/1.1657530 (1969).

32 Abe, M., Gomi, M., Shōno, K., Mori, Y. & Nomura, S. A Method for Measuring the Direction Angle of a Magnetization with a Vibrating Sample Magnetometer: Application to $SmFeO_3$ in the Spin Reorientation Region. *Jpn. J. Appl. Phys.* **16**, 279-282, doi:10.1143/jjap.16.279 (1977).

33 Tsymbal, L. T., Kamenev, V. I., Bazaliy, Y. B., Khara, D. A. & Wigen, P. E. Structural properties of $ErFeO_3$ in the spin-reorientation region. *Phys. Rev. B* **72**, 052413, doi:10.1103/PhysRevB.72.052413 (2005).

34 Bazaliy, Y. B., Tsymbal, L. T., Kakazei, G. N., Izotov, A. I. & Wigen, P. E. Spin-reorientation in $ErFeO_3$ Zero-field transitions, three-dimensional phase diagram, and anisotropy of erbium magnetism. *Phys. Rev. B* **69**, 104429, doi:10.1103/PhysRevB.69.104429 (2004).

35 Berini, B. *et al.* High temperature phase transitions and critical exponents of Samarium orthoferrite determined by in situ optical ellipsometry. *J. Appl. Phys.* **111**, 053923, doi:10.1063/1.3692088 (2012).

36 Kimel, A. V., Kirilyuk, A., Tsvetkov, A., Pisarev, R. V. & Rasing, T. Laser-induced ultrafast spin reorientation in the antiferromagnet $TmFeO_3$. *Nature* **429**, 850-853, doi:10.1038/nature02659 (2004).

37 Saito, K., Sato, A., Bhattacharjee, A. & Sorai, M. High-precision detection of the heat-capacity anomaly due to spin reorientation in $TmFeO_3$ and $HoFeO_3$. *Solid State Commun.* **120**, 129-132, doi:https://doi.org/10.1016/S0038-1098(01)00359-3 (2001).

38 Saito, K. *et al.* Heat-capacity anomaly due to spin reorientation and thermodynamic functions of $ErFeO_3$ and $TmFeO_3$. *J. Magn. Magn. Mater.* **225**, 381-388, doi:https://doi.org/10.1016/S0304-8853(00)01268-3 (2001).

39 Tan, Z. *et al.* Charge disproportionation and interchange transitions in twelve-layer $BaFeO_3$. *Phys. Rev. B* **102**, 054404, doi:10.1103/PhysRevB.102.054404 (2020).

40 Avci, S. *et al.* Magnetically driven suppression of nematic order in an iron-based superconductor. *Nat. Commun.* **5**, 3845, doi:10.1038/ncomms4845 (2014).

41 Waßer, F. *et al.* Spin reorientation in $Ba_{0.65}Na_{0.35}Fe_2As_2$ studied by single-crystal neutron diffraction. *Phys. Rev. B* **91**, 060505, doi:10.1103/PhysRevB.91.060505 (2015).

42 Song, Y. *et al.* Spin anisotropy due to spin-orbit coupling in optimally hole-doped $Ba_{0.67}K_{0.33}Fe_2As_2$. *Phys. Rev. B* **94**, 214516, doi:10.1103/PhysRevB.94.214516 (2016).

43 Whangbo, M. H., Gordon, E. E., Xiang, H., Koo, H. J. & Lee, C. Prediction of Spin Orientations in Terms of HOMO-LUMO Interactions Using Spin-Orbit Coupling as Perturbation. *Acc. Chem. Res.* **48**, 3080-3087, doi:10.1021/acs.accounts.5b00408 (2015).

44 Sessoli, R., Gatteschi, D., Caneschi, A. & Novak, M. A. Magnetic bistability in a metal-ion cluster. *Nature* **365**, 141-143, doi:10.1038/365141a0 (1993).

45 Thorarinsdottir, A. E. & Harris, T. D. Metal–Organic Framework Magnets. *Chem. Rev.* **120**, 8716-8789, doi:10.1021/acs.chemrev.9b00666 (2020).

46 Goodwin, C. A. P., Ortu, F., Reta, D., Chilton, N. F. & Mills, D. P. Molecular magnetic hysteresis at 60 kelvin in dysprosocenium. *Nature* **548**, 439-442, doi:10.1038/nature23447 (2017).

47 Goodwin, C. A. P. Blocking like it's hot: a synthetic chemists' path to high-temperature lanthanide single molecule magnets. *Dalton Trans.* **49**, 14320-14337, doi:10.1039/D0DT01904F (2020).

48 Kawaguchi, S. *et al.* High-throughput powder diffraction measurement system consisting of multiple MYTHEN detectors at beamline BL02B2 of SPring-8. *Rev. Sci. Instrum.* **88**, 085111, doi:10.1063/1.4999454 (2017).

49 Izumi, F. & Momma, K. Three-Dimensional Visualization in Powder Diffraction. *Solid State Phenom.* **130**, 15-20, doi:10.4028/www.scientific.net/SSP.130.15 (2007).

Figures

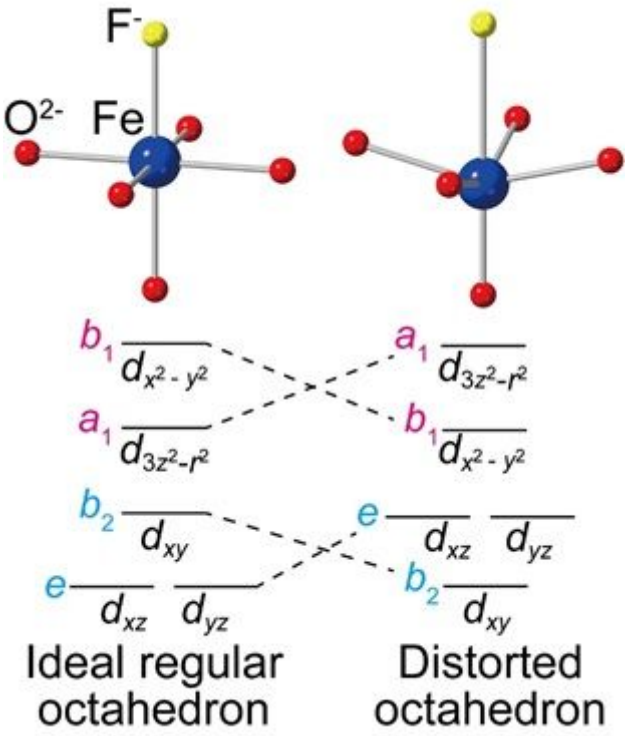

Figure 1

The crystal field energies of 3d orbital in ideal regular and distorted octahedra of FeO5F. While the ideal FeO6 octahedron has the Oh symmetry, the ligand replacement by F– stabilizes d3z2–r2, dxz, and dyz orbitals (left). On the other hand, ferroelectric-like distortion stabilizes t dx2–y2 and dxy orbitals and could induce level crossing.

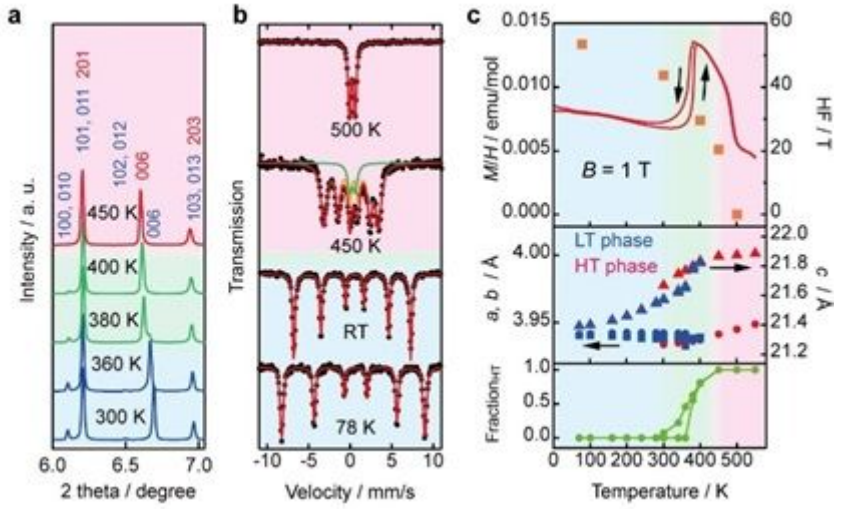

Figure 2

Structural and magnetic transitions of Pb3Fe2O5F2 at high temperatures. a, Temperature evolution of synchrotron X-ray diffraction pattern (= 0.41967 Å) on heating. The blue and red annotations indicate the index of peaks for the LT (aP × aP × cP) and HT (2aP × 2aP × cP) phases, respectively, clearly demonstrating the two-phase coexistence at 380 K. b, Temperature evolution of the 57Fe Mössbauer spectra, all fitted well with a Lorentzian function. c, Temperature dependences of (top) the magnetic susceptibility and hyperfine field (HF), (middle) the nomalized lattice parameters (middle), and (bottom) the fraction of the HT phase.

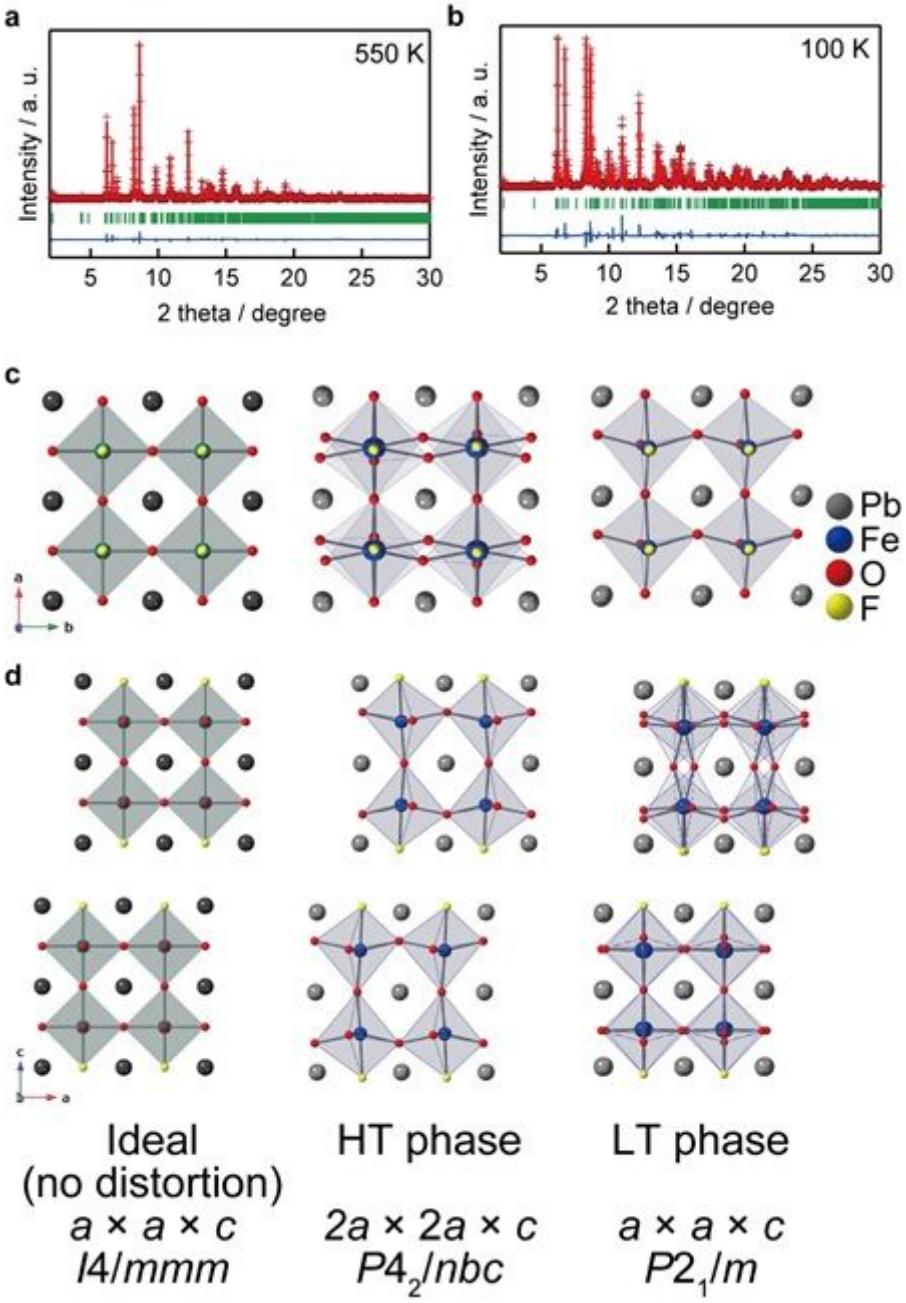

Figure 3

Structural refinement of Pb3Fe2O5F2 for the LT and HT phases. Results of Rietveld refinement of the SXRD data and the refined structures at (a) 550 K and (b) 100 K (λ = 0.41967 Å). Red crosses, solid black lines, and solid blue lines represent the observed, calculated, and difference intensities, respectively. Green ticks indicate the Bragg peak positions. Stacking of the perovskite double layer viewed along the c (c) and b (d) axes, for the ideal (left) , HT (middle), and (right) LT phases.

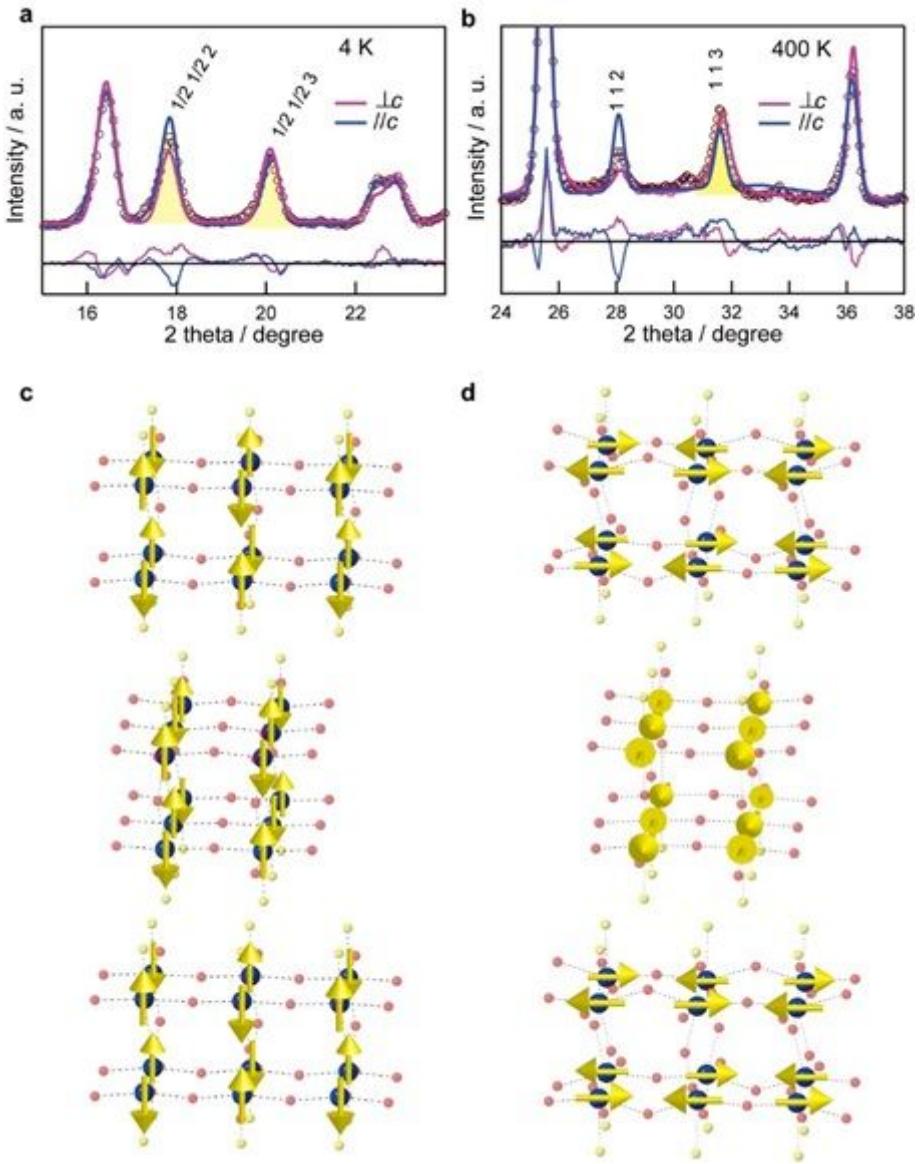

Figure 4

Spin reorientation in Pb3Fe2O5F2. The magnetic reflections in the NPD patterns and the magnetic structures for the (a, c) LT (4 K with λ = 1.5366 Å) and (b, d) HT (400 K with λ = 2.4068 Å) phases. Profiles are shown with Rietveld refinement assuming G-type antiferromagnetic order with ⊥c (red) and //c (blue) spin orientations. The bottom lines in a and b are the difference between observed and calculated intensities for each orientation. The change in the intensity ratio of the magnetic peaks indicates spin reorientation occurs simultaneously with the structural transition.

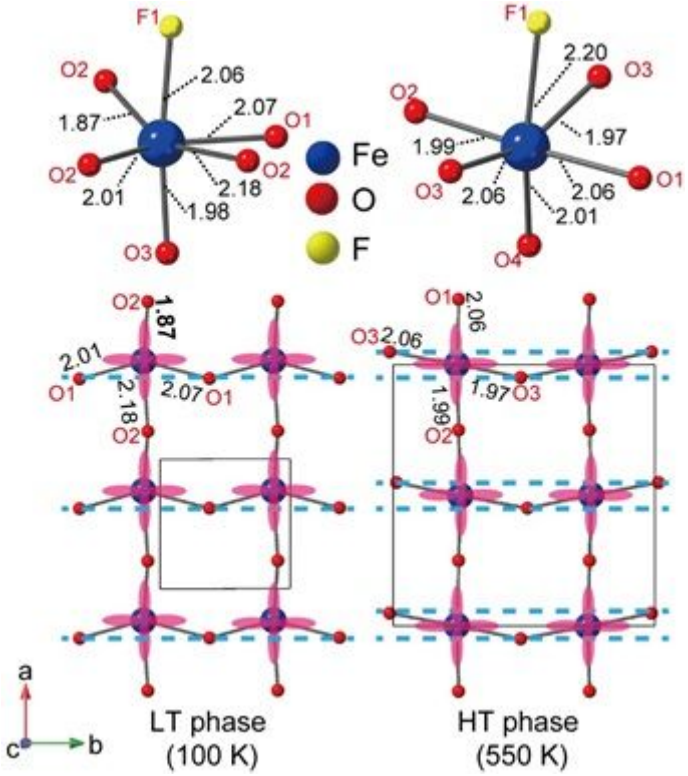

Figure 5

Stabilized dx2-y2 orbital induced by changes in local coordination around Fe3+ between the LT and HT phases. The annotated figures indicate bond lengths in Å scale. (upper) Refined local structures of the FeO5F octahedron of the LT (100 K) and HT (550 K) phases. The local coordination changes anisotropically by the structural transition. (lower) FeO2 place along the ab plane. The pink shades denote dx2–y2 orbital of Fe3+ and solid lines represent the unit cells. The alignment of O ions changes from (left) zigzag to (right) liner manner along the b axis.

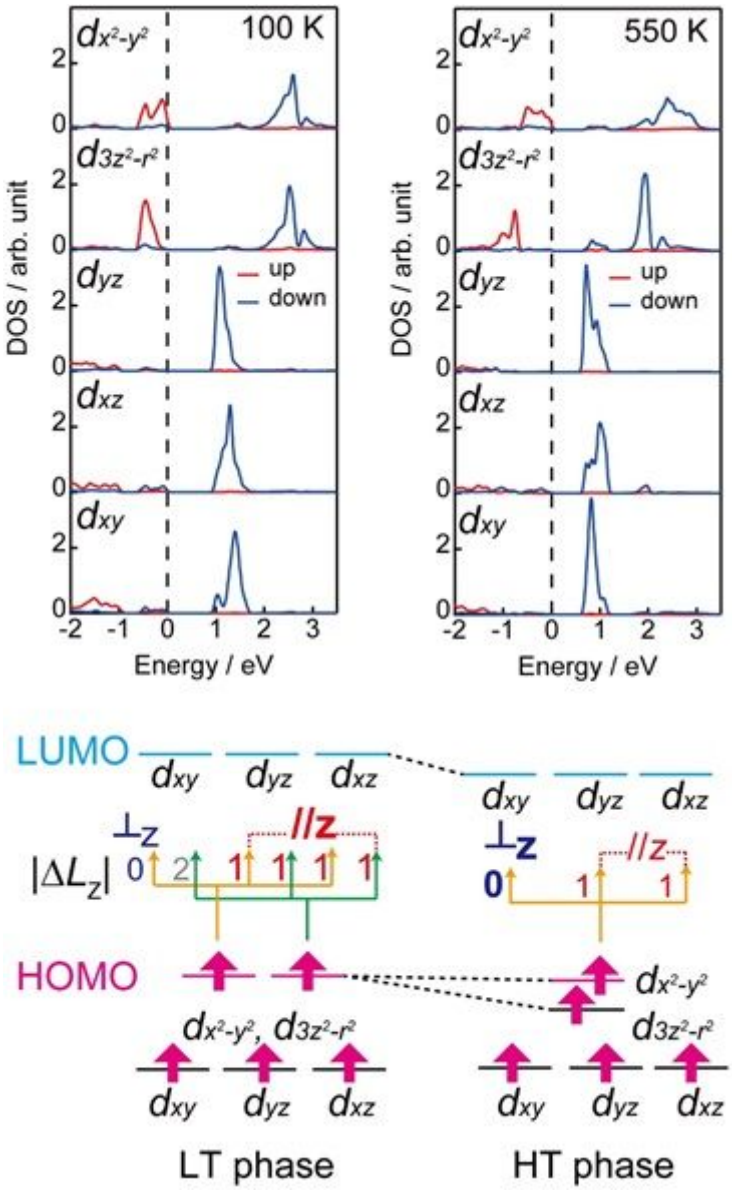

Figure 6

Altered magnetic HOMO-LUMO interaction by the structural transition. (upper) Partial density of states (DOS) of Fe3+ for the HT and LT phase. (lower) Schematic diagram illustrates how SR occurs in Pb3Fe2O5F2. Energy diagrams of 3d orbital in FeIIIO5F octahedra for the LT and HT phases are shown with magnetic HOMO, LUMO, and corresponding |ΔLZ|. The |ΔLZ| = 0 and 1 interactions for 3d5 electronic configuration give ⊥c and //c orientations, respectively.

Supplementary Files

This is a list of supplementary files associated with this preprint. Click to download.

- SI3.pdf